Flexible integrated photonics: where materials, mechanics and optics meet [Invited]

Juejun Hu,[1,*] Lan Li,[1] Hongtao Lin,[1] Ping Zhang,[1] Weidong Zhou,[2,4] and Zhenqiang Ma [3,5]

[1]*Department of Materials Science and Engineering, University of Delaware, Newark, DE 19716, USA*
[2]*Department of Electrical Engineering, NanoFAB Center, University of Texas at Arlington, Texas 76019, USA*
[3]*Department of Electrical and Computer Engineering, University of Wisconsin-Madison, Wisconsin 53706, USA*
[4]*wzhou@uta.edu*
[5]*mazq@engr.wisc.edu*
[*]*hujuejun@udel.edu*

Abstract: While the vast majority of integrated photonic devices are traditionally fabricated on rigid substrates, photonic integration of both passive and active photonic devices on flexible polymer substrates has been demonstrated in recent years, and its applications in imaging, sensing and optical interconnects are being actively pursued. This paper presents an overview of the emerging field of mechanically flexible photonics, where we examine material processing and mechanical design rationales dictated by application-specific optical functionalities. The examples include semiconductor nanomembranes which serve as the key enabling material for hybrid inorganic-organic flexible active photonics, and monolithically integrated passive photonic structures fabricated from semiconductors, polymers, or amorphous materials. Technical challenges and further research opportunities related to materials engineering and device integration on flexible substrates are also discussed.

OCIS codes: (160.3130) Integrated optics materials; (160.6000) Semiconductor materials; (160.2750) Glass and other amorphous materials; (130.3120) Integrated optics devices; (140.4780) Optical resonators; (040.5160) Photodetectors; (350.3850) Materials processing.

References and links

1. W. Zhou, Z. Ma, H. Yang, Z. Qiang, G. Qin, H. Pang, L. Chen, W. Yang, S. Chuwongin, and D. Zhao, "Flexible photonic-crystal Fano filters based on transferred semiconductor nanomembranes," J. Phys. D **42**(23), 234007 (2009).
2. H. C. Ko, M. P. Stoykovich, J. Song, V. Malyarchuk, W. M. Choi, C.-J. Yu, J. B. Geddes 3rd, J. Xiao, S. Wang, Y. Huang, and J. A. Rogers, "A hemispherical electronic eye camera based on compressible silicon optoelectronics," Nature **454**(7205), 748–753 (2008).
3. L. Zhou, A. Wanga, S. Wu, J. Sun, S. Park, and T. Jackson, "All-organic active matrix flexible display," Appl. Phys. Lett. **88**(8), 083502 (2006).
4. E. Bosman, G. Van Steenberge, B. Van Hoe, J. Missinne, J. Vanfleteren, and P. Van Daele, "Highly Reliable Flexible Active Optical Links," IEEE Photon. Technol. Lett. **22**(5), 287–289 (2010).
5. D. Guidotti, Y. Jianjun, M. Blaser, V. Grundlehner, and G. Chang, "Edge viewing photodetectors for strictly in-plane lightwave circuit integration and flexible optical interconnects," in *Proceedings of 56th Electronic Components and Technology Conference* (IEEE, 2006), pp. 782–788.
6. T. Shibata and A. Takahashi, "Flexible opto-electronic circuit board for in-device interconnection," in *Proc. 58th Electron. Compon. Technol. Conf.* (IEEE, 2008), pp. 261–267.
7. B. Swatowski, C. Amb, S. Breed, D. Deshazer, W. Ken Weidner, R. Dangel, N. Meier, and B. Offrein, "Flexible, stable, and easily processable optical silicones for low loss polymer waveguides," Proc. SPIE **8622**, 8622–8624 (2013).
8. K. Cherenack, K. V. Os, and L. V. Pieterson, "Smart photonic textiles begin to weave their magic," Laser Focus World **48**, 63–66 (2012).
9. Z. Yu, X. Niu, Z. Liu, and Q. Pei, "Intrinsically stretchable polymer light-emitting devices using carbon nanotube-polymer composite electrodes," Adv. Mater. **23**(34), 3989–3994 (2011).

#191249 - $15.00 USD Received 31 May 2013; revised 31 Jul 2013; accepted 2 Aug 2013; published 12 Aug 2013

10. J. Yoon, L. Li, A. V. Semichaevsky, J. H. Ryu, H. T. Johnson, R. G. Nuzzo, and J. A. Rogers, "Flexible concentrator photovoltaics based on microscale silicon solar cells embedded in luminescent waveguides," Nat Commun **2**, 343 (2011).
11. J. Yoon, A. J. Baca, S. I. Park, P. Elvikis, J. B. Geddes 3rd, L. Li, R. H. Kim, J. Xiao, S. Wang, T. H. Kim, M. J. Motala, B. Y. Ahn, E. B. Duoss, J. A. Lewis, R. G. Nuzzo, P. M. Ferreira, Y. Huang, A. Rockett, and J. A. Rogers, "Ultrathin silicon solar microcells for semitransparent, mechanically flexible and microconcentrator module designs," Nat. Mater. **7**(11), 907–915 (2008).
12. W. Park and J. Lee, "Mechanically tunable photonic crystal structure," Appl. Phys. Lett. **85**(21), 4845–4847 (2004).
13. Y. Chen, H. Li, and M. Li, "Flexible and tunable silicon photonic circuits on plastic substrates," Sci Rep **2**, 622 (2012).
14. C. L. Yu, H. Kim, N. de Leon, I. W. Frank, J. T. Robinson, M. McCutcheon, M. Liu, M. D. Lukin, M. Loncar, and H. Park, "Stretchable photonic crystal cavity with wide frequency tunability," Nano Lett. **13**(1), 248–252 (2013).
15. D. Taillaert, W. Paepegem, J. Vlekken, and R. Baets, "A thin foil optical strain gage based on silicon-oninsulator microresonators," Proc. SPIE **6619**, 661914, 661914-4 (2007).
16. L. Fan, L. T. Varghese, Y. Xuan, J. Wang, B. Niu, and M. Qi, "Direct fabrication of silicon photonic devices on a flexible platform and its application for strain sensing," Opt. Express **20**(18), 20564–20575 (2012).
17. J. C. Martinez-Anton, H. Canabal, J. A. Quiroga, E. Bernabeu, M. A. Labajo, and V. C. Testillano, "Enhancement of surface inspection by Moiré interferometry using flexible reference gratings," Opt. Express **8**(12), 649–654 (2001).
18. L. Ge, X. Wang, H. Chen, K. Qiu, and S. Fu, "Flexible subwavelength gratings fabricated by reversal soft UV nanoimprint," Chin. Opt. Lett. **10**(9), 090502–090505 (2012).
19. D. H. Kim, N. Lu, R. Ma, Y. S. Kim, R. H. Kim, S. Wang, J. Wu, S. M. Won, H. Tao, A. Islam, K. J. Yu, T. I. Kim, R. Chowdhury, M. Ying, L. Xu, M. Li, H. J. Chung, H. Keum, M. McCormick, P. Liu, Y. W. Zhang, F. G. Omenetto, Y. Huang, T. Coleman, and J. A. Rogers, "Epidermal electronics," Science **333**(6044), 838–843 (2011).
20. Z. Ma, "Materials science:An electronic second skin," Science **333**(6044), 830–831 (2011).
21. S. Ahn and L. Guo, "High-speed roll-to-roll nanoimprint lithography on flexible plastic substrates," Adv. Mater. **20**(11), 2044–2049 (2008).
22. J. Ok, H. Youn, M. Kwak, K. Lee, Y. Shin, L. Guo, A. Greenwald, and Y. Liu, "Continuous and scalable fabrication of flexible metamaterial films via roll-to-roll nanoimprint process for broadband plasmonic infrared filters," Appl. Phys. Lett. **101**(22), 223102 (2012).
23. C. Choi, L. Lin, Y. Liu, J. Choi, L. Wang, D. Haas, J. Magera, and R. T. Chen, "Flexible optical waveguide film fabrications and optoelectronic devices integration for fully embedded board-level optical interconnects," J. Lightwave Technol. **22**(9), 2168–2176 (2004).
24. Y. Huang, G. Paloczi, A. Yariv, C. Zhang, and L. Dalton, "Fabrication and replication of polymer integrated optical devices using electron-beam lithography and soft lithography," J. Phys. Chem. B **108**(25), 8606–8613 (2004).
25. G. Paloczi, Y. Huang, and A. Yariv, "Free-standing all-polymer microring resonator optical filter," Electron. Lett. **39**(23), 1650–1651 (2003).
26. K. J. Kim, J. K. Seo, and M. C. Oh, "Strain induced tunable wavelength filters based on flexible polymer waveguide Bragg reflector," Opt. Express **16**(3), 1423–1430 (2008).
27. J. Clark and G. Lanzani, "Organic photonics for communications," Nat. Photonics **4**(7), 438–446 (2010).
28. K. J. Kim, J. W. Kim, M. C. Oh, Y. O. Noh, and H. J. Lee, "Flexible polymer waveguide tunable lasers," Opt. Express **18**(8), 8392–8399 (2010).
29. T. Lu, L. Chiu, P. Lin, and P. Lee, "One-dimensional photonic crystal nanobeam lasers on a flexible substrate," Appl. Phys. Lett. **99**(7), 071101 (2011).
30. S. Furumi, H. Fudouzi, H. Miyazaki, and Y. Sakka, "Flexible polymer colloidal -crystal lasers with a light-emitting planar defect," Adv. Mater. **19**(16), 2067–2072 (2007).
31. H. Song, M. Oh, S. Ahn, W. Steier, H. R. Fetterman, and C. Zhang, "Flexible low voltage electro-optic polymer modulators," Appl. Phys. Lett. **82**(25), 4432–4434 (2003).
32. K. S. Novoselov, D. Jiang, F. Schedin, T. J. Booth, V. V. Khotkevich, S. V. Morozov, and A. K. Geim, "Two-dimensional atomic crystals," Proc. Natl. Acad. Sci. U.S.A. **102**(30), 10451–10453 (2005).
33. J. A. Rogers, M. G. Lagally, and R. G. Nuzzo, "Synthesis, assembly and applications of semiconductor nanomembranes," Nature **477**(7362), 45–53 (2011).
34. H. Lin, L. Li, Y. Zou, O. Ogbuu, S. Danto, J. D. Musgraves, K. Richardson, and J. Hu, "Chalcogenide glass planar photonics: from mid-IR sensing to 3-D flexible substrate integration," Proc. SPIE **8600**, 8600–8620 (2013).
35. C. Hsueh, "Modeling of elastic deformation of multilayers due to residual stresses and external bending," J. Appl. Phys. **91**(12), 9652–9656 (2002).
36. D. H. Kim, J. H. Ahn, W. M. Choi, H. S. Kim, T. H. Kim, J. Song, Y. Y. Huang, Z. Liu, C. Lu, and J. A. Rogers, "Stretchable and foldable silicon integrated circuits," Science **320**(5875), 507–511 (2008).
37. Y. Maeda and Y. Hashiguchi, "Flexible film waveguides with excellent bending properties," Proc. SPIE **6899**, 68990D, 68990D-8 (2008).

#191249 - $15.00 USD Received 31 May 2013; revised 31 Jul 2013; accepted 2 Aug 2013; published 12 Aug 2013

38. W. Yang, H. Yang, G. Qin, Z. Ma, J. Berggren, M. Hammar, R. Soref, and W. Zhou, "Large-area InP-based crystalline nanomembrane flexible photodetectors," Appl. Phys. Lett. **96**(12), 121107 (2010).
39. W. Zhou, M. Zhenqiang, C. Santhad, Y. Shuai, J. Seo, D. Zhao, H. Yang, and W. Yang, "Semiconductor nanomembranes for integrated silicon photonics and flexible photonics," Opt. Quantum Electron. **44**(12-13), 605–611 (2012).
40. L. Li, H. Lin, Y. Zou, and J. Hu, Department of Materials Science and Engineering, University of Delaware, Newark, DE 19716, and S. Qiao, N. Lu, S. Danto, J. D. Musgraves, and K. Richardson are preparing a manuscript to be called "3-D integrated flexible glass photonics."
41. D. H. Kim, N. Lu, R. Ghaffari, Y. S. Kim, S. P. Lee, L. Xu, J. Wu, R. H. Kim, J. Song, Z. Liu, J. Viventi, B. de Graff, B. Elolampi, M. Mansour, M. J. Slepian, S. Hwang, J. D. Moss, S. M. Won, Y. Huang, B. Litt, and J. A. Rogers, "Materials for multifunctional balloon catheters with capabilities in cardiac electrophysiological mapping and ablation therapy," Nat. Mater. **10**(4), 316–323 (2011).
42. R. Verplancke, F. Bossuyt, D. Cuypers, and J. Vanfleteren, "Thin-film stretchable electronics technology based on meandering interconnections: fabrication and mechanical performance," J. Micromech. Microeng. **22**(1), 015002 (2012).
43. D. Kim and J. A. Rogers, "Stretchable electronics: Materials strategies and devices," Adv. Mater. **20**(24), 4887–4892 (2008).
44. S. Mack, M. A. Meitl, A. J. Baca, Z. T. Zhu, and J. A. Rogers, "Mechanically flexible thin-film transistors that use ultrathin ribbons of silicon derived from bulk wafers," Appl. Phys. Lett. **88**(21), 213101 (2006).
45. X. Xu, H. Subbaraman, A. Hosseini, C. Y. Lin, D. Kwong, and R. T. Chen, "Stamp printing of silicon-nanomembrane-based photonic devices onto flexible substrates with a suspended configuration," Opt. Lett. **37**(6), 1020–1022 (2012).
46. M. A. Meitl, Z. T. Zhu, V. Kumar, K. J. Lee, X. Feng, Y. Y. Huang, I. Adesida, R. G. Nuzzo, and J. A. Rogers, "Transfer printing by kinetic control of adhesion to an elastomeric stamp," Nat. Mater. **5**(1), 33–38 (2006).
47. M. J. Zablocki, A. Sharkawy, O. Ebil, and D. W. Prather, "Nanomembrane transfer process for intricate photonic device applications," Opt. Lett. **36**(1), 58–60 (2011).
48. A. Ghaffari, A. Hosseini, X. Xu, D. Kwong, H. Subbaraman, and R. T. Chen, "Transfer of micro and nano-photonic silicon nanomembrane waveguide devices on flexible substrates," Opt. Express **18**(19), 20086–20095 (2010).
49. D. Chanda, K. Shigeta, S. Gupta, T. Cain, A. Carlson, A. Mihi, A. J. Baca, G. R. Bogart, P. Braun, and J. A. Rogers, "Large-area flexible 3D optical negative index metamaterial formed by nanotransfer printing," Nat. Nanotechnol. **6**(7), 402–407 (2011).
50. D. Hines, V. Ballarotto, E. Williams, Y. Shao, and S. Solin, "Transfer printing methods for the fabrication of flexible organic electronics," J. Appl. Phys. **101**(2), 024503 (2007).
51. H. C. Yuan, M. M. Roberts, P. Zhang, B. N. Park, L. J. Klein, D. E. Savage, F. S. Flack, Z. Ma, P. G. Evans, M. A. Eriksson, G. K. Celler, and M. G. Lagally, "Silicon-based nanomembrane materials: the ultimate in strain engineering," in *Topical Meeting on Silicon Monolithic Integrated Circuits in RF Systems (SiRF)*, San Diego, CA, 2006, pp. 327–333.
52. H. C. Yuan and Z. Ma, "Microwave thin-film transistors using Si nanomembranes on flexible polymer substrate," Appl. Phys. Lett. **89**(21), 212105 (2006).
53. H. C. Yuan, Z. Ma, M. M. Roberts, D. E. Savage, and M. G. Lagally, "High-speed strained-single-crystal-silicon thin-film transistors on flexible polymers," J. Appl. Phys. **100**(1), 013708 (2006).
54. H. C. Yuan, G. K. Celler, and Z. Ma, "7.8-GHz flexible thin-film transistors on a low-temperature plastic substrate," J. Appl. Phys. **102**(3), 034501 (2007).
55. K. Zhang, J. Seo, W. Zhou, and Z. Ma, "Fast flexible electronics using transferrable silicon nanomembranes (Topical Review)," J. Phys. D. **45**(14), 143001 (2012).
56. Z. Ma and L. Sun, "Will future RFIC be flexible?(Invited)," in *IEEE 10th Annual Wireless and Microwave Technology Conference, 2009. WAMICON '09.*, Clearwater, FL, 2009, pp. 1–5.
57. L. Sun, G. Qin, G. K. Celler, W. Zhou, and Z. Ma, "12-GHz thin-film transistors with transferrable silicon nanomembranes for high-performance massive flexible electronics," Small **6**, 2553–2557 (2010).
58. H. Yang, Z. Qiang, H. Pang, Z. Ma, and W. D. Zhou, "Surface-normal fano filters based on transferred silicon nanomembranes on glass substrates," Electron. Lett. **44**(14), 858–859 (2008).
59. L. Chen, Z. Qiang, H. Yang, H. Pang, Z. Ma, and W. D. Zhou, "Polarization and angular dependent transmissions on transferred nanomembrane Fano filters," Opt. Express **17**(10), 8396–8406 (2009).
60. Z. Qiang, H. Yang, L. Chen, H. Pang, Z. Ma, and W. Zhou, "Fano filters based on transferred silicon nanomembranes on plastic substrates," Appl. Phys. Lett. **93**(6), 061106 (2008).
61. W. Yang, S. Chuwongin, D. Zhao, H. Yang, Z. Ma, and W. Zhou, "Flexible solar cells based on stacked semiconductor nanomembranes on plastic substrates," in *CLEO* San Jose, CA, 2010.
62. S. Chuwongin, W. Yang, H. Yang, W. D. Zhou, and Z. Ma, "Flexible Crystalline InP Nanomembrane LED Arrays," in *IEEE Photonics Society Annual Meeting* Denver, CO, 2010.
63. H. Zhou, J.-H. Seo, D. M. Paskiewicz, Y. Zhu, G. K. Celler, P. M. Voyles, W. Zhou, M. G. Lagally, and Z. Ma, "Fast flexible electronics with strained silicon nanomembranes," Sci Rep **3**, 1291 (2013).
64. Y. Zou, D. Zhang, H. Lin, L. Li, L. Moreel, J. Zhou, Q. Du, O. Ogbuu, K. Dobson, R. Birkmire, and J. Hu, Department of Materials Science and Engineering, University of Delaware, Newark, DE 19716, and S. Danto, J.

#191249 - $15.00 USD Received 31 May 2013; revised 31 Jul 2013; accepted 2 Aug 2013; published 12 Aug 2013

D. Musgraves, and K. Richardson are preparing a manuscript to be called “High-Performance, High-Index-Contrast Chalcogenide Glass Photonics on Silicon and Unconventional Nonplanar Substrates.”
65. S. Aksu, M. Huang, A. Artar, A. A. Yanik, S. Selvarasah, M. R. Dokmeci, and H. Altug, “Flexible Plasmonics on Unconventional and Nonplanar Substrates,” Adv. Mater. **23**(38), 4422–4430 (2011).
66. H. Park, A. Fang, S. Kodama, and J. Bowers, “Hybrid silicon evanescent laser fabricated with a silicon waveguide and III-V offset quantum wells,” Opt. Express **13**(23), 9460–9464 (2005).
67. J. E. Bowers, H. Park, A. W. Fang, O. Cohen, R. Jones, and M. Paniccia, “Design and fabrication of optically pumped hybrid silicon-AlGaInAs evanescent lasers,” IEEE J. Sel. Top. Quantum Electron. **12**(6), 1657–1663 (2006).
68. O. G. Schmidt and K. Eberl, “Nanotechnology. Thin solid films roll up into nanotubes,” Nature **410**(6825), 168 (2001).
69. S. A. Scott and M. G. Lagally, “Elastically strain-sharing nanomembranes: flexible and transferable strained silicon and silicon–germanium alloys,” J. Phys. D Appl. Phys. **40**(4), R75–R92 (2007).
70. J. A. Rogers, Z. Bao, K. Baldwin, A. Dodabalapur, B. Crone, V. R. Raju, V. Kuck, H. Katz, K. Amundson, J. Ewing, and P. Drzaic, “Paper-like electronic displays: Large-area rubber-stamped plastic sheets of electronics and microencapsulated electrophoretic inks,” Proc. Natl. Acad. Sci. U.S.A. **98**(9), 4835–4840 (2001).
71. H. Ma, A. K.-Y. Jen, and L. Dalton, “Polymer-based optical waveguides: materials, processing, and devices,” Adv. Mater. **14**(19), 1339–1365 (2002).
72. S. Shibata, M. Horiguchi, K. Jinguji, S. Mitachi, T. Kanamori, and T. Manabe, “Prediction of loss minima in infra-red optical fibers,” Electron. Lett. **17**(21), 775–777 (1981).
73. B. Rangarajan, A. Y. Kovalgin, K. Wörhoff, and J. Schmitz, “Low-temperature deposition of high-quality silicon oxynitride films for CMOS-integrated optics,” Opt. Lett. **38**(6), 941–943 (2013).
74. J. T. Choy, J. D. Bradley, P. B. Deotare, I. B. Burgess, C. C. Evans, E. Mazur, and M. Lončar, “Integrated TiO_2 resonators for visible photonics,” Opt. Lett. **37**(4), 539–541 (2012).
75. N. Carlie, J. D. Musgraves, B. Zdyrko, I. Luzinov, J. Hu, V. Singh, A. Agarwal, L. C. Kimerling, A. Canciamilla, F. Morichetti, A. Melloni, and K. Richardson, “Integrated chalcogenide waveguide resonators for mid-IR sensing: Leveraging material properties to meet fabrication challenges,” Opt. Express **18**(25), 26728–26743 (2010).
76. J. Sandland, “Sputtered silicon oxynitride for microphotonics: a materials study,” Ph.D. thesis, Massachusetts Institute of Technology (2005).
77. J. Kim, C. Florea, K. A. Winick, and M. McCoy, “Design and fabrication of low-loss hydrogenated amorphous silicon overlay DBR for glass waveguide devices,” IEEE J. Sel. Top. Quantum Electron. **8**(6), 1307–1315 (2002).
78. D. P. Birnie, “Rational solvent selection strategies to combat striation formation during spin coating of thin films,” J. Mater. Res. **16**(04), 1145–1154 (2001).
79. Y. Zou, H. Lin, O. Ogbuu, L. Li, S. Danto, S. Novak, J. Novak, J. D. Musgraves, K. Richardson, and J. Hu, “Effect of annealing conditions on the physio-chemical properties of spin-coated As_2Se_3 chalcogenide glass films,” Opt. Mater. Express **2**(12), 1723–1732 (2012).
80. Y. Zha, S. Fingerman, S. Cantrell, and C. Arnold, “Pore formation and removal in solution-processed amorphous arsenic sulfide films,” J. Non-Cryst. Solids **369**, 11–16 (2013).
81. L. Schares, J. Kash, F. Doany, C. Schow, C. Schuster, D. Kuchta, P. Pepeljugoski, J. Trewhella, C. Baks, R. John, L. Shan, Y. Kwark, R. Budd, P. Chiniwalla, F. Libsch, J. Rosner, C. Tsang, C. Patel, J. Schaub, R. Dangel, F. Horst, B. Offrein, D. Kucharski, D. Guckenberger, S. Hegde, H. Nyikal, C. Lin, A. Tandon, G. Trott, M. Nystrom, D. Bour, M. Tan, and D. Dolfi, “Terabus: terabit/second-class card-level optical interconnect technologies,” IEEE J. Sel. Top. Quantum Electron. **12**(5), 1032–1044 (2006).
82. R. Bockstaele, M. De Wilde, W. Meeus, H. Sergeant, O. Rits, J. Van Campenhout, J. De Baets, P. Van Daele, F. Dorgeuille, S. Eitel, M. Klemenc, R. Annen, J. Van Koetsem, J. Goudeau, B. Bareel, R. Fries, P. Straub, F. Marion, J. Routin, and R. Baets, “Chip-to-chip parallel optical interconnects over optical backpanels based on arrays of multimode waveguides,” Proc. Symp. IEEE/LEOS 61–64 (2004).
83. D. Butler, M. Li, S. Li, K. Matthews, V. Nazarov, A. Koklyushkin, R. McCollum, Y. Geng, and J. Luther, “Multicore optical fiber and connectors for high bandwidth density, short reach optical links,” presented at the IEEE Optical Interconnects Conference, 5–8 May 2013.
84. L. Li, Y. Zou, H. Lin, and J. Hu, Department of Materials Science and Engineering, University of Delaware, Newark, DE 19716, and X. Sun, N. Feng, S. Danto, K. Richardson, T. Gu, and M. Haney are preparing a manuscript to be called “A fully-integrated flexible photonic platform for chip-to-chip optical interconnects.”
85. P. Horak, W. Stewart, and W. H. Loh, “Continuously tunable optical buffer with a dual silicon waveguide design,” Opt. Express **19**(13), 12456–12461 (2011).
86. B. Bhola, H. Song, H. Tazawa, and W. Steier, “Polymer microresonator strain sensors,” IEEE Photon. Technol. Lett. **17**(4), 867–869 (2005).
87. J. Hu, N. Carlie, N. N. Feng, L. Petit, A. Agarwal, K. Richardson, and L. C. Kimerling, “Planar waveguide-coupled, high-index-contrast, high-Q resonators in chalcogenide glass for sensing,” Opt. Lett. **33**(21), 2500–2502 (2008).
88. I. M. Pryce, K. Aydin, Y. A. Kelaita, R. M. Briggs, and H. A. Atwater, “Highly strained compliant optical metamaterials with large frequency tunability,” Nano Lett. **10**(10), 4222–4227 (2010).

#191249 - $15.00 USD Received 31 May 2013; revised 31 Jul 2013; accepted 2 Aug 2013; published 12 Aug 2013

89. S. Olcum, A. Kocabas, G. Ertas, A. Atalar, and A. Aydinli, "Tunable surface plasmon resonance on an elastomeric substrate," Opt. Express **17**(10), 8542–8547 (2009).
90. Y. M. Song, Y. Xie, V. Malyarchuk, J. Xiao, I. Jung, K. J. Choi, Z. Liu, H. Park, C. Lu, R. H. Kim, R. Li, K. B. Crozier, Y. Huang, and J. A. Rogers, "Digital cameras with designs inspired by the arthropod eye," Nature **497**(7447), 95–99 (2013).
91. T. Kim, R. H. Kim, and J. A. Rogers, "Microscale inorganic light-emitting diodes on flexible and stretchable substrates," IEEE Photon. J. **4**(2), 607–612 (2012).
92. T. I. Kim, Y. H. Jung, J. Song, D. Kim, Y. Li, H. S. Kim, I. S. Song, J. J. Wierer, H. A. Pao, Y. Huang, and J. A. Rogers, "High-efficiency, microscale GaN light-emitting diodes and their thermal properties on unusual substrates," Small **8**(11), 1643–1649 (2012).
93. R. H. Kim, H. Tao, T. I. Kim, Y. Zhang, S. Kim, B. Panilaitis, M. Yang, D. H. Kim, Y. H. Jung, B. H. Kim, Y. Li, Y. Huang, F. G. Omenetto, and J. A. Rogers, "Materials and designs for wirelessly powered implantable light-emitting systems," Small **8**(18), 2812–2818 (2012).
94. T. I. Kim, J. G. McCall, Y. H. Jung, X. Huang, E. R. Siuda, Y. Li, J. Song, Y. M. Song, H. A. Pao, R. H. Kim, C. Lu, S. D. Lee, I. S. Song, G. Shin, R. Al-Hasani, S. Kim, M. P. Tan, Y. Huang, F. G. Omenetto, J. A. Rogers, and M. R. Bruchas, "Injectable, cellular-scale optoelectronics with applications for wireless optogenetics," Science **340**(6129), 211–216 (2013).
95. S. W. Hwang, H. Tao, D. H. Kim, H. Cheng, J. K. Song, E. Rill, M. A. Brenckle, B. Panilaitis, S. M. Won, Y. S. Kim, Y. M. Song, K. J. Yu, A. Ameen, R. Li, Y. Su, M. Yang, D. L. Kaplan, M. R. Zakin, M. J. Slepian, Y. Huang, F. G. Omenetto, and J. A. Rogers, "A physically transient form of silicon electronics," Science **337**(6102), 1640–1644 (2012).

1. Introduction

Flexible integrated photonics generally refers to photonic devices fabricated on flexible polymer substrates which can be mechanically deformed (bending, folding, rolling, twisting, stretching or compression) without compromising their optical performance [1]. Mechanical flexibility is the key attribute of these devices enabling emerging applications such as flexible imaging/display arrays [2, 3], short-reach optical links [4–7], wearable photonic textiles [8, 9], solar cells [10, 11], broadband tunable photonic devices [12–14], strain gauges [15, 16], and optical systems conformally integrated on curved surfaces [17, 18] or biological tissues [19, 20]. Flexible substrate integration also potentially enables low-cost, large-area device fabrication via roll-to-roll (R2R) processing [21, 22].

The requirement of mechanical flexibility poses unique constraints on the material processing and mechanical engineering of flexible photonic devices in addition to their optical design considerations. Polymers have long been a preferred material for flexible photonic devices given their inherent mechanical flexibility. Besides serving as the flexible substrate material, polymers are also used for waveguiding [23, 24], filtering [25, 26], light emission [27–30], and optical modulation [31]. Besides polymers, new materials are progressively being introduced onto flexible platforms to offer new functionalities. Many of these materials are traditionally regarded as rigid or even brittle in their bulk form; however, free-standing nanomembranes made of the same materials can be tightly bent without cracking, since surface strain induced by bending is inversely proportional to the membrane thickness. In particular, semiconductor nanomembranes (NMs) present an attractive material platform for active photonic device integration on polymer substrates [32, 33]. Semiconductor NMs retain a single crystalline structure essential for efficient optoelectronic device operation, while their small thickness imparts large mechanical flexibility, a salient feature that their bulk counterparts usually do not possess. The mechanical design rationale aiming to reduce strain level in flexible photonic devices is also applied to other material systems. One example is the recent demonstration of highly flexible, high-index-contrast glass-based photonic devices [34].

In this article, we present an overview of the rapidly developing field of flexible integrated photonics in light of the latest material and mechanical design innovations. The paper is organized as follows: we first examine the mechanical design principles that enable large mechanical flexibility in planar photonic structures and the material selection criteria for active and passive photonic components. Device designs and processing methods defined by

#191249 - $15.00 USD Received 31 May 2013; revised 31 Jul 2013; accepted 2 Aug 2013; published 12 Aug 2013

these general principles as well as specific application needs are subsequently reviewed. Finally we conclude with a discussion on the emerging trends and opportunities in this field.

2. Nano-mechanical engineering: the path towards ultimate mechanical flexibility

Mechanical flexibility, measured by the maximum possible deformation (bending radius, relative elongation, etc.) without structurally damaging the photonic devices, is determined by yield strengths of materials that constitute the device as well as the device geometry which specifies the strain exerted on the devices during deformation. Therefore, the basic design recipe for improving flexibility is to minimize the strain of the photonic device layer at a given mechanical deformation configuration. This is particularly important for photonic devices made of rigid materials such as semiconductors or glasses. Here we will focus on the design strategies to enhance mechanical flexibility of photonic devices when they undergo two categories of deformation: bending/folding/rolling/twisting (note that twisting of a thin, non-stretchable membrane is equivalent to single-axis bending) and stretching/compression.

2.1. Design approaches to increase bending flexibility of photonic structures

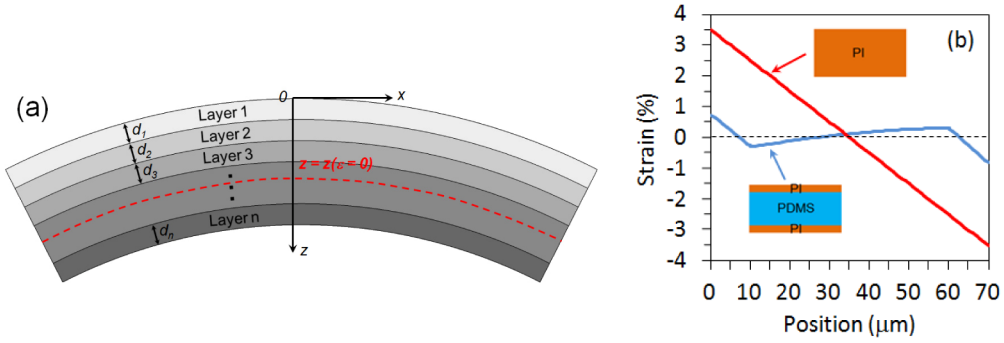

Fig. 1. (a) Pure bending of a multi-layer structure, whose the top and bottom surfaces undergo tensile and compressive strain, respectively. The neutral plane position is specified by Eq. (1). Strains vanishes at the neutral plane, and thus maximum bending flexibility is achieved when the photonic devices are located at the plane; (b) finite element simulated through-thickness strain distribution in structures bent to a radius of 1 mm: the blue curve corresponds to strain in a polyimide (10 μm)-silicone (50 μm)-polyimide (10 μm) tri-layer structure, and the red curve plots strain in a single polyimide layer of the same total thickness (70 μm). The large, three-orders-of-magnitude modulus mismatch between silicone and polyimide results in significant shear strain in silicone which invalidates Eq. (1) and effectively relieves the strain on the multi-layer stack surfaces.

In the case of simple bending, strain minimization can be attained by adopting the so-called "neutral plane" configuration. At the neutral plane, the strain vanishes. Therefore, positioning thin film photonic devices at the neutral plane inside a multi-layer stack minimizes their strains during bending. For a multi-layer stack with the 1st layer on top and the n^{th} layer at the bottom (Fig. 1), the neutral plane position from the top surface is given by:

$$z(\varepsilon = 0) = \sum_{i=1}^{n} E_i d_i \left[\left(\sum_{j=1}^{i} d_j \right) - \frac{d_i}{2} \right] \Bigg/ \sum_{i=1}^{n} E_i d_i \qquad (1)$$

where E_i and d_i are the modulus and thickness of the i^{th} layer, respectively. The equation assumes linear mechanics, pure bending, and no-slip boundaries between the layers, which suggests zero shear deformation in the layers [35]. These assumptions are usually valid in the case of small bending (bending radius $r \gg \sum_{i=1}^{n} d_i$). Based on the simple bending theory, elastic strain in the stack linearly increases with the distance away from the neutral plane. As a result, nanomembrane devices with an ultra-thin layout contribute to significantly reduced

#191249 - $15.00 USD Received 31 May 2013; revised 31 Jul 2013; accepted 2 Aug 2013; published 12 Aug 2013

strain when they are strategically positioned at the neutral plane location. This approach has been successfully applied to demonstrate foldable silicon electronic circuits [36] and polymer waveguides with improved bending properties [37].

According to Eq. (1), the neutral plane design requires the photonic elements to be embedded inside the multi-layer structure. While such a configuration is generally compatible with electronic circuits, it may not meet the fabrication requirements or application needs of integrated photonics. For example, encapsulating the photonic components deep underneath a thick top cladding layer prohibits evanescent wave interactions with the external environment which is essential for chem-bio sensing and evanescent optical coupling. One solution to this challenge is to fabricate photonic devices on the top surface of a relatively thin (< 50 μm) flexible substrate with low elastic modulus, which reduces the strain level in the device layer according to the multi-layer bending theory despite that the device layer is not aligned with the neutral plane [35]. This approach has been most frequently implemented in conjunction with transfer printing of semiconductor NMs [1, 38, 39] and typically allows bending with > 10 mm radius. Further improved bending flexibility can be achieved by engineering the multi-layer structure. It is worth noting that Eq. (1) may become invalid due to the elastic modulus mismatch between layers in the case of large bending (i.e. small bending radius). For example, when an elastomer layer with low Young's modulus (~MPa) is sandwiched between two glassy polymer layers with much higher moduli (~GPa), large shear deformation takes place in the elastomer layer to minimize elastic deformation energy in the two rigid glassy polymer layers. Figure 1(b) and 1(c) illustrates such an example where a 50 μm thick silicone elastomer layer (E = 2 MPa) is sandwiched between two polyimide (PI) layers (E = 2.5 GPa) of 10 μm thickness each to form a tri-layer structure. When bent, the silicone layer practically decouples the in-plane strain in the two PI layers and serves as an effective strain relieving agent which reduces the strain in on the multi-layer stack surface by a factor of 5 compared to that in a single PI layer of the same thickness (Fig. 1(b)). We have recently employed this mechanical design to demonstrate highly flexible (minimum bending radius < 0.5 mm) photonic devices made of chalcogenide glasses, despite the poor mechanical strength of the glass materials [40].

2.2. Stretchable photonics: lessons learnt from stretchable electronics

Mechanical stretching and compression offers a convenient way for broadband tuning of the operation wavelengths of photonic devices [13]. In addition, the ability to accommodate stretching is necessary for photonic sensor systems integrated with biological tissues [41]. Stretching and compression are distinctively different from bending in that there is no "neutral plane" during deformation, and thus the aforementioned vertical ("out-of-plane") multi-layer stack engineering approach does not apply. However, the same design rationale of reducing strain at critical points when the devices locate still holds. Local strain in the devices resulting from stretching can be suppressed through in-plane patterning of the photonic structures. Interconnect lines used in stretchable electronics on elastomer substrates provide an excellent example for the design principle. While the metal material constituting the interconnects is hardly stretchable, metal lines patterned into serpentine shapes are able to withstand large elongation without fracture [41]: the mechanism is similar to that of stretching a helix shaped spring. Introducing a polymer material with higher Young's modulus than the elastomer substrate as a support for the meandering lines can further improve robustness of the structure [42]. This design approach is readily applicable to produce stretchable photonic wire waveguides, which can be used to connect photonic components fabricated on stiff, non-stretchable islands. Other geometries, such as wavy buckled structures [43], may also be used to create stretchable components from stiff materials.

#191249 - $15.00 USD Received 31 May 2013; revised 31 Jul 2013; accepted 2 Aug 2013; published 12 Aug 2013

3. Material selection and processing for flexible photonics

From the previous section, we note that through ingenious geometry designs, the deformation capacity of photonic structures can be decoupled from its constituent material's mechanical properties. The insight allows designers to focus on fabrication compatibility and optical properties of materials in the material down selection process for flexible photonic devices. To date, most flexible photonic components are fabricated either using transfer printing or direct monolithic patterning. In this section, we will first discuss the two processing routes. Material design options will then be evaluated based on processing constraints and device functional requirements for two main components of a flexible photonic circuit: passive photonics and active optoelectronics.

3.1. Transfer printing of semiconductor nanomembrane structures and devices

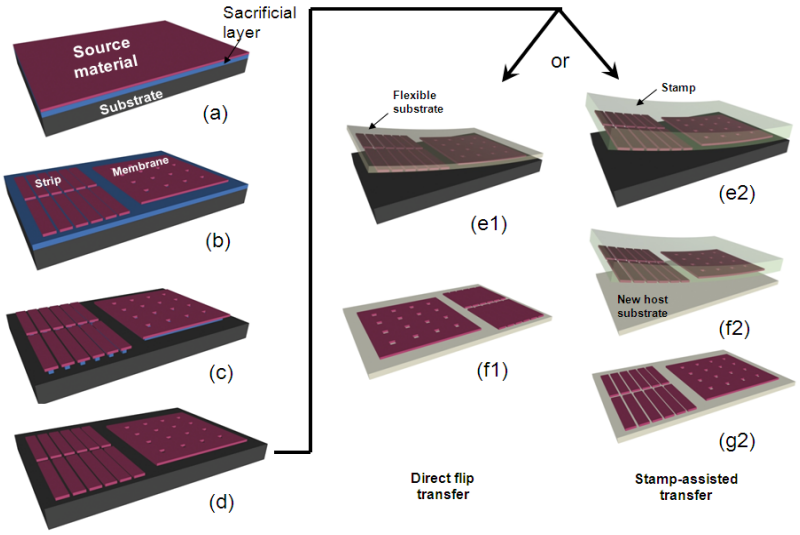

Fig. 2. General process illustration for crystalline semiconductor membrane release, transfer and stacking. (a) Begin with source material (e.g., SOI, GeOI, III-V multi layers with a sacrificial layer). Metallization can be applied here, if needed. (b) Pattern top layer into membrane (or strip forms) down to the sacrificial layer. (c) Release membrane by undercutting the sacrificial layer. (d) Fully released membrane settles down on the handling substrate via van der Waals force ("in-place bonding"). *Direct flip transfer:* (e1). Apply glue on host (e.g., flexible) substrate and attach it to the handling substrate. (f1) Lift-up the host substrate and flip to complete the transfer. Glue can be dissolved if needed. *Stamp-assisted transfer:* (e2) Bring a stamp (e.g., Polydimethylsiloxane, or PDMS) toward the handling substrate, press and lift-up. (f2) Apply the stamp with membrane attached to a new host substrate (which can be coated with glue, but not necessary). (g2) Slowly peel off the stamp or remove the stamp with shear force, leaving the membrane to stay on the new host substrate. Multiple layers can be applied by repeating (a)-(f1) or (a)-(g2).

Transfer printing, alternatively termed stamp printing, has several variants but all of them involve release of the functional layers (e.g. crystalline semiconductor NMs) or structures (e.g. fabricated devices) from the starting substrate, and transfer of the functional layers or structures onto a foreign flexible substrate. Figure 2 shows a general transfer printing process flow. The source material (e.g., SOI, GeOI, III-V multi layers with a sacrificial layer) is first being patterned into membrane (or strip forms) down to the sacrificial layer (Fig. 2(a)-2(b)). Top membrane layers are then released by undercutting the sacrificial layer (Fig. 2(c)), with fully released membrane settles down on the handling substrate via van der Waals force (Fig. 2(d)) (note: this in-place bonding case only applies to thin sacrificial layers. For thick ones, please refer to another paper from Rogers' group [44]). The wet etch step either completely

#191249 - $15.00 USD Received 31 May 2013; revised 31 Jul 2013; accepted 2 Aug 2013; published 12 Aug 2013

releases the devices, which subsequently settle down and are weakly bonded to the silicon substrate via van der Waals force, or partially undercut the supporting oxide layer beneath the devices to form pedestal structures. The latter method prevents lateral shift of devices during the wet etch process [13, 45]. Finally membrane transfer process can take place with either a *direct flip transfer* or *stamp-assisted transfer* processes (Fig. 2(e)-2(f)). In the *direct flip transfer* process, an adhesion layer is applied on the host (foreign) substrate first. The membrane to be transferred can be picked up by the host substrate directly to complete the transfer. The adhesion layer (e.g., glue) can be dissolved afterwards, if needed. In the *stamp-assisted transfer* process, a stamp (e.g., PDMS) was used to press toward the handling substrate, and lift-up the membrane to be transferred. Then the membrane attached to the stamp was picked up and attached to a new host substrate, which can be coated with glue, if needed. Slowly peeling off the stamp or removing the stamp with shear force, the NM can be left on the new host substrate [46].

By releasing high-quality flexible materials from SOI and other source substrates and transfer-printing them to a new host substrate, integration of dissimilar material systems becomes feasible on both rigid and flexible substrates, with individually optimized material structures, energy-efficient and flexible integration process, and intelligent functions. The transfer-printing steps can also be repeated to produce stacked multi-layer photonic structures [47]. Besides Si [48], many materials including III-V semiconductors [38, 39], metals [49], and organic semiconductors [50] are all amenable to transfer printing processing.

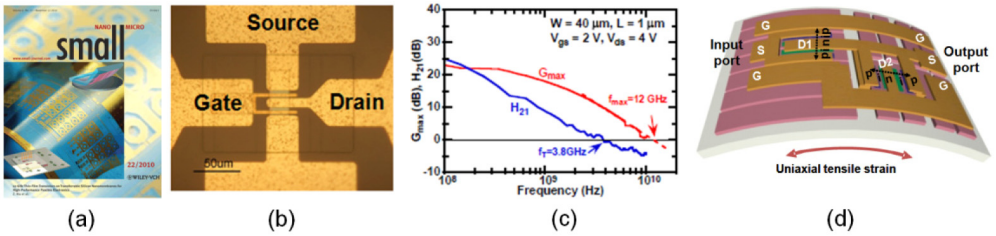

Fig. 3. Flexible RF transistors and switches: (a) An array of 12 GHz Si-NM-based thin-film transistor integrated with passives on a bent plastic substrate (Cover page on journal *Small*, Nov. 20, 2010; image courtesy of [57]); (b) An optical image of the fabricated device, with channel length 1.0 um; (c) Measured device speed figures of merit; and (d) Flexible 20 GHz RF switches.

Based on transfer printed NMs on flexible substrates, various high performance photonic and optoelectronic devices have been demonstrated, including flexible photodetectors, LEDs, and solar cells, flexible Si Fano resonance filters, and mostly significantly, fast flexible electronics, with record speed of RF performances, owing to high electron mobility in single crystalline semiconductors [51–62]. Many excellent results have also been reported by Lagally *et al*. [51, 53, 69] and Rogers *et al*. [33, 41, 43] on the unique electronic, photonic, and thermoelectronic, and mechanical properties associated with this new class of inorganic flexible semiconductor membrane material system. To improve the yield of the printing transfer process, Xu *et al.* reported an innovative stamp printing technique with an adhesion controllable suspended configuration [45]. To address the alignment challenge over the large area flexible substrate, a local alignment scheme in combination with more accurate Si-NM transfer measures for minimizing alignment errors was reported [57]. By realizing 1 μm channel alignment for the Si-NMs on a soft plastic substrate, thin film transistors with a record speed of 12 GHz maximum oscillation frequency were demonstrated (Fig. 3). Recently, based on the strained Si/SiGe/Si-NMs transferred onto flexible substrates, another record was set for fast flexible transistors, with maximum oscillation frequency of 15 GHz demonstrated [63]. These results indicate the great potential of properly processed Si-NMs for high-performance flexible optoelectronics [55].

#191249 - $15.00 USD Received 31 May 2013; revised 31 Jul 2013; accepted 2 Aug 2013; published 12 Aug 2013

High quality photonic crystal (PhC) structures have been successfully transferred onto PET substrates based on NM transfer processes, as shown in Fig. 4. PhC air hole structures were first fabricated with the target wavelength of 1550 nm on 260-nm thick silicon-on-insulator (SOI) wafers using e-beam lithography and plasma dry-etching processes. Shown in Fig. 4(a) are a schematic (top) and scanning electron micrographs (SEMs, bottom) of the patterned PhC SOI structures, respectively. The patterned PhC SOI structures were subsequently immersed in aqueous diluted HF solution (49% HF: DI water = 1:4) for several hours to etch away the BOX (buried oxide) layer selectively (Fig. 4(b)). Once the top patterned PhC Si-NM was completely released, it was rinsed in DI water and transferred onto PET plastic substrates (Fig. 4(c)). A micrograph is shown in Fig. 4(iv), where a large piece of NM was transferred onto a flexible (curved) PET substrate.

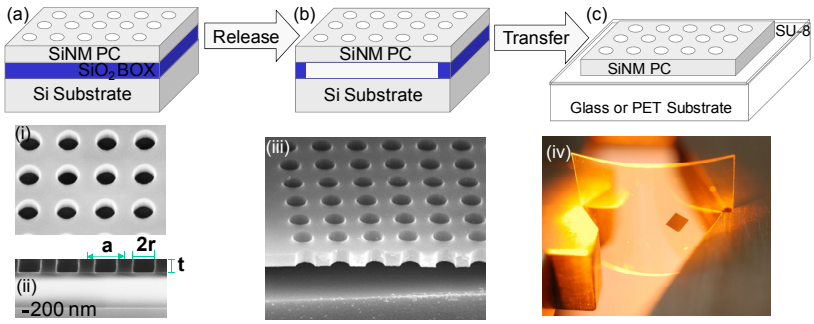

Fig. 4. Modified process for air hole PhC NM structure transfer. Single layer NM pattern (a), release (b), and transfer (c) process, along with experimental results (bottom): (i) SEM image of top and (ii) cross-sectional view of patterned Si-NM on SOI, (iii) SEM images of patterned Si-NM after BHF etching of BOX layer underneath the pattern area, (iv) a micrograph of a 3 × 3 mm patterned NM transferred onto 1x1" flexible PET substrate (image courtesy of [1]).

3.2. Monolithic integration on plastic substrates

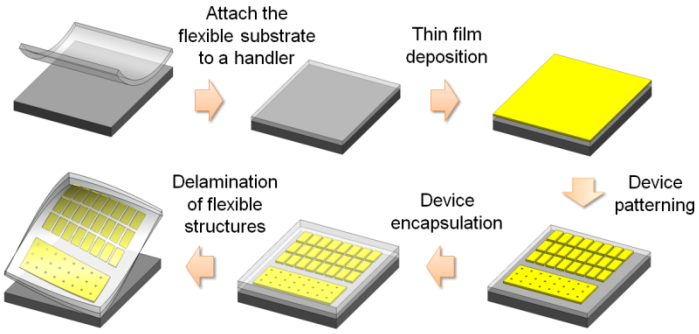

Fig. 5. Fabrication process flow for monolithically integrated flexible photonic devices: the flexible substrate is first attached to a rigid substrate for ease of handling, followed by optical film deposition and patterning to form the device structures. The encapsulated devices are peeled off from the rigid handler to complete the fabrication process.

Compared to the hybrid transfer printing approach, direct monolithic patterning of *passive* photonic devices on flexible substrates offers a much simplified alternative with improved yield, large-area patterning capability, and potential compatibility with roll-to-roll processing. The typical process flow of monolithic photonic device fabrication on plastic substrates is schematically illustrated in Fig. 5. The flexible polymer substrate is first attached to a rigid handler substrate to facilitate handling in subsequent processing steps, followed by deposition of the thin film device layer via Physical Vapor Deposition (PVD), Chemical Vapor Deposition (CVD), or solution processing (spin-coating and dip-coating). It is critical to

#191249 - $15.00 USD Received 31 May 2013; revised 31 Jul 2013; accepted 2 Aug 2013; published 12 Aug 2013

ensure the flatness and low roughness of the substrate and film surfaces, since surface height variation can lead to defocus and image distortion during projection lithography, or stitching error during electron beam lithography. Patterning of the thin film into functional photonic structures is accomplished through plasma etching (note that the RF power should be kept low to reduce plasma damage to the polymer substrate [16]), lift-off [34, 40], nanoimprint [64], or nanostencil lithography [65]. The monolithic fabrication route has been applied to create optical waveguides, resonators, gratings, and plasmonic nanostructures on flexible substrates. As an example, an optical micrograph of a micro-ring resonator fabricated using thermal nanoimprint in As_2Se_8 glass films on a PET plastic substrate is shown in Fig. 6(b) [64]. The process starts with making a master for stamp fabrication, which comprises thermally reflowed photoresist lines on a rigid substrate with atomically smooth surfaces. PDMS stamps which inherit the smooth surface finish were fabricated via replica molding, and the photoresist master can be repeatedly used for PDMS stamp fabrication. Photonic devices on flexible substrates were subsequently patterned using single-step nanoimprint at temperatures above the As_2Se_8 glass transition temperature. The method produced high-index-contrast photonic waveguide structures with a low RMS surface roughness of ~1 nm and optical propagation loss as low as 0.8 dB/cm, comparable to the performance of state-of-the-art devices on traditional semiconductor substrates.

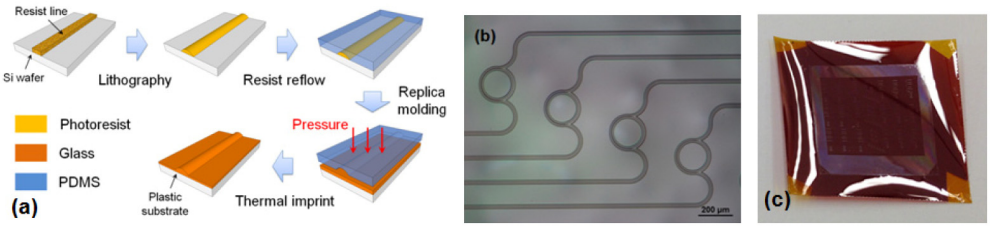

Fig. 6. (a) Single step thermal nanoimprint direct patterning process on plastic substrates; (b) optical micrograph of As_2Se_8 chalcogenide glass micro-ring resonators fabricated on a PET plastic substrate using imprint. The color variation is due to thickness non-uniformity of the PET substrate; (c) photo of chalcogenide glass resonator devices printed on a flexible substrate. The device shows a loaded Q factor of 10^4.

3.3. Materials design considerations for flexible photonics

Heterogeneous integration is currently the most promising approach to high performance photonic devices (also applicable to high-speed electronics), considering the difficulty to engineer indirect bandgap materials (in particular, Si). This argument is evidenced by the recent successes on the hybrid Si evanescent laser, the photonic devices based on the InP-bonding-to-Si structure [66, 67].

With recent advances in nanostructured material systems, the enabling materials for flexible photonics have expanded into inorganic crystalline and hybrid material systems, such as semiconductor quantum dots, nanowires, tubes, and thin film NMs on flexible substrates. Inorganic crystalline semiconductor NMs (free-standing sheets with nanometer to sub-micrometer scale thicknesses) have, in the last several years, demonstrated great potential to become a disruptive technology, driven primarily by the successes shown with Group IV crystalline NMs transferred and stacked onto foreign substrates, including both rigid (e.g. silicon and glass) and flexible (e.g. plastics and polymers) substrates. The drivers for this potential are the inherently novel electronic and mechanical properties of these sheets; their flexibility, conformability, biocompatibility, and transferability to other hosts; the ability to introduce strain (and thus novel properties associated with strain) in ways not possible with bulk materials; and the ability to integrate membranes of different materials because of the much better bondability of membranes than bulk material.

#191249 - $15.00 USD Received 31 May 2013; revised 31 Jul 2013; accepted 2 Aug 2013; published 12 Aug 2013

Owing to the stackability of nanomembranes based on PDMS transfer printing processes, originally developed by Rogers *et al.* [46], heterogeneous integration of dissimilar materials becomes very promising without compromising their structural integrity and optical properties. Since active optoelectronic components, in particular light emitters such as LEDs and lasers generally require using pristine single crystal materials to suppress defect-assisted carrier recombination, this unique feature justifies transfer printing as the processing route of choice for active optoelectronic device fabrication. High quality single crystalline Si-NMs have been transferred onto various foreign substrates, such as glass, flexible PET (polyethylene terephthalate) plastics, etc., based on low temperature transfer and stacking processes, developed by various groups [51–54, 68–70].

In contrast, optical properties, rather than electronic or optoelectronic properties underlie the material choice for most passive photonic devices. Three types of materials are currently being explored for passive photonic components on plastic substrates: optical polymers, single crystal semiconductors, and inorganic amorphous materials, as all of them can fulfill the basic requirement of low optical loss for passive applications. Optical polymers, in particular fluorinated polymers, exhibit low optical loss down to 0.01 dB/cm in the 1310/1550 nm telecommunication wave bands [71]. In addition, polymers are highly versatile for device processing: polymer waveguides can be fabricated using conventional lithography and etching, direct photo patterning, micro-molding, or imprint/embossing, and they are fully compatible with plastic substrate integration. However, polymer materials by themselves generally offer relatively low index contrast. In comparison, single crystalline semiconductor NMs and inorganic amorphous materials possess high refractive indices suitable for high-density integration, and both types of materials have been used for low-loss flexible planar passive device fabrication [13, 16, 40, 45, 55]. Since passive applications do not require perfect crystallinity, amorphous materials feature unique processing and integration advantages over their single-crystalline counterparts: they are known to exhibit very low optical loss [72], and can be monolithically integrated on polymer substrates free of lattice matching constraints. Multi-layer vertically integrated photonic structures can be readily fabricated as well by multiple sequential deposition and lithographic patterning steps with superior throughput and alignment accuracy [34]. It is important to choose a deposition process whose thermal budget is compatible with the polymer substrate material. For example, low temperature Plasma Enhanced Chemical Vapor Deposition (PECVD) was used to deposit a-Si films on heat stabilized polyester substrates at 200 °C for flexible photonic strain sensor fabrication [16]. The low CVD deposition temperature, however, compromised the optical quality of films and partially accounts for the high optical loss (~100 dB/cm) in the fabricated devices. A recent paper by Rangarajan *et al.* reported the deposition of low-loss (< 3 dB/cm) silicon oxynitride films via PECVD at 150 °C, which suggests a possible new route for high-performance flexible passive photonic device fabrication provided that plasma damage to the polymer substrate can be somehow circumvented [73]. Evaporation and sputtering are among the most common PVD deposition techniques, and amorphous transition metal oxides (e.g. TiO_2 [74]) and chalcogenide glasses [75] are both amenable to these low-temperature PVD deposition methods. It is worth noting that sputtering deposited Si_3N_4 and a-Si films exhibit high optical losses due to presence of silicon dangling bonds and are thus not suitable for flexible photonics applications [76, 77]. Finally, solution processing (sol-gel, spin-coating, dip-coating, etc.) offers promising low-cost, large-area alternatives to PVD and CVD deposition techniques, although optical attenuation resulting from residual solvents and microstructure inhomogeneity needs to be mitigated through careful processing optimization [78–80].

4. Flexible photonic devices: function dictates form

A broad spectrum of photonic structures and devices integrated on flexible substrates have been demonstrated using the aforementioned fabrication techniques. In this section, we

#191249 - $15.00 USD Received 31 May 2013; revised 31 Jul 2013; accepted 2 Aug 2013; published 12 Aug 2013

highlight several device application examples where mechanical flexibility either constitutes the key feature enabling the target applications, or contributes to significantly improved device performance.

4.1. Optical links for board-level interconnects

The ever increasing need for high-bandwidth data traffic between computer chips in High Performance Computing (HPC) has pushed electrical interconnects to their functional limit. Several optical interconnect schemes have been demonstrated as potential solutions to resolve this "interconnect bottleneck". The examples include designs based on on-board polymer waveguide interconnects (i.e. the "optoelectronic printed circuit board" configuration) [81], multi-mode fiber ribbons [82] or multi-core fibers [83], and flexible optical waveguides [4–7]. Since chips are usually assembled onto the circuit board using "pick-and-place" surface mounting technologies which have limited spatial placement accuracy (typically in the order of 10 μm or larger), mechanical flexibility of optical interconnects is essential to accommodate the limited chip-to-chip relative positioning accuracy. Compared to other approaches, flexible optical interconnects also allow significant deployment flexibility and scalability to ultra-high bandwidth density.

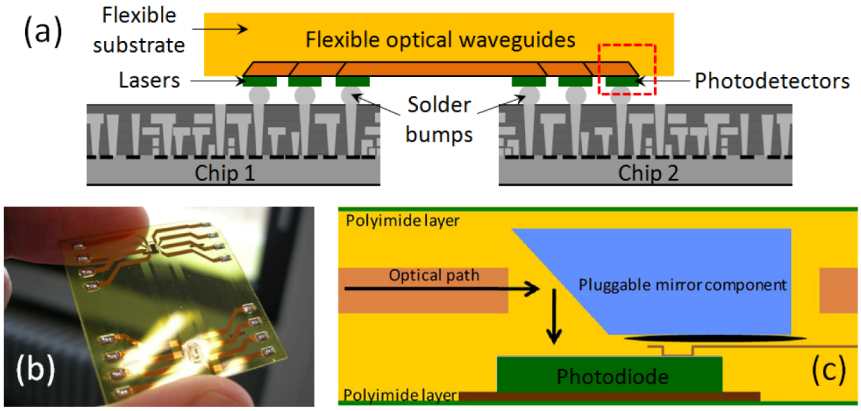

Fig. 7. (a) Schematic cross-sectional structure of an embodiment of fully-integrated flexible optical link for chip-to-chip interconnects, which consists of an array of optical waveguides on a common flexible substrate as well as active components (lasers and detectors) bonded onto the flexible substrate and optically coupled to the waveguides; (b) photo of a prototypical flexible optical link (image courtesy of [4]); (c) schematic view of the optical link shown in Fig. 7(b) with embedded waveguides, micro-mirrors, and optoelectronic components (image courtesy of [4]).

Figure 7(a) schematically illustrates the cross-sectional structure of a fully-integrated flexible chip-to-chip optical link [84]. The link consists of an array of optical waveguides on a common flexible substrate as well as active optoelectronic components (lasers and detectors) bonded onto the flexible substrate and optically coupled to the waveguides. Two ends of the flexible link is flip-chip bonded and electrically connected to chips through solder bumps and on-chip metal vias. Bosman *et al.* demonstrated a prototypical flexible optical link by integrating commercial GaAs VCSELs and photodiodes with a flexible polymer waveguide foil (Fig. 7(b) and 7(c)). Guidotti *et al.* fabricated and tested flexible optical waveguide interconnects directly coupled to edge-viewing lasers photodetectors [5]. Since the optical link only interfaces with the chips electronically, no optical alignment is required during packaging. In this sense, the flexible optical interconnects can be viewed as the planar counterpart of active optical cables, although their planar design offers much higher data bandwidth scalability to well beyond 10 Tbps, as the interconnect bandwidth density is only limited by the physical sizes of on-chip contact pads and solder bumps, and not by the limited

#191249 - $15.00 USD Received 31 May 2013; revised 31 Jul 2013; accepted 2 Aug 2013; published 12 Aug 2013

optical alignment accuracy or optical coupler size. Reach of such planar flexible optical links, however, is ultimately limited by optical waveguide loss. IBM and Dow Corning recently reported flexible polymer waveguides with optical losses as low as 0.05 dB/cm, which is adequate for chip-to-chip and even board-to-board interconnects [7].

4.2. Broadband tunable photonic devices

Flexible photonics offers a unique platform to exploit optomechanical coupling in integrated photonics systems, and realize broadband photonic tuning where the wavelength tuning rage far exceeds what can possibly be achieved using conventional electro-optic or themo-optic tuning. The optomechanical coupling originates from two mechanisms: the material response characterized by strain-optic coefficients $dn/d\varepsilon$, and the device shape change as a result of mechanical deformation. For instance, optomechanical coupling manifests itself as resonant wavelength shift $d\lambda$ in a resonant cavity under mechanical strain ε [16]:

$$\frac{d\lambda}{d\varepsilon} = \sum_i \left[\frac{\lambda}{n_g} \cdot \Gamma_i \cdot \left(\frac{dn}{d\varepsilon} \right)_i \right] + \frac{n_{eff}}{n_g} \cdot \frac{\lambda}{L} \cdot \frac{dL}{d\varepsilon} + \frac{\lambda}{n_g} \cdot \frac{dn_{eff}}{d\varepsilon} \qquad (2)$$

where Γ_i and $(dn/d\varepsilon)_i$ are the optical confinement factor and strain-optic coefficient in the i th cavity material, L is the cavity length, and n_g and n_{eff} denote the group index and effective indices, respectively. In Eq. (2), the first term on the right hand side (RHS) represents the photoelastic (i.e. strain-optic) *material* response, the second term manifests the cavity *length* change, and the third term results from the cavity *cross-sectional geometry* modification. Compared to the original formalism used in Ref. 16, Eq. (2) separates the contributions from materials and cross-section geometry change. As an example of the latter effect, optical properties of a coupled waveguide system can be efficiently tuned through varying the gap width between the two coupled waveguides [85].

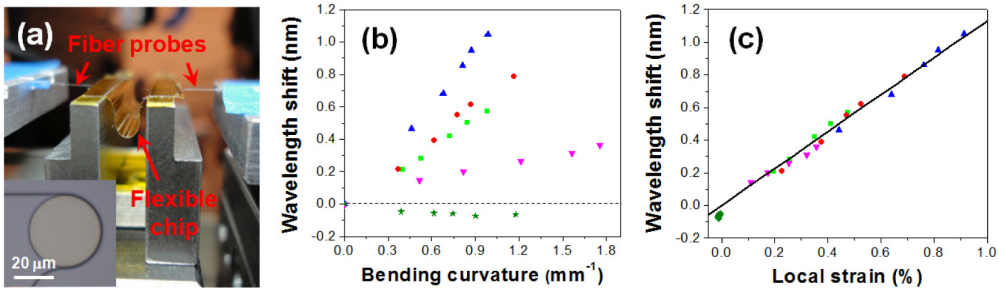

Fig. 8. (a) Photo of a flexible resonator sample chip under testing: optical transmission through the bus waveguides is monitored *in situ* using fiber end fire coupling as the flexible chip is bent; inset shows the top-view optical micrograph of a pullery-coupled [87] micro-disk resonator fabricated on a flexible substrate; (b) micro-disk resonant wavelength shift induced by bending of the flexible chip: dots of each color are data points collected on one sample, and the resonator top/bottom cladding layer thickness combinations were varied among different samples, which resulted in the different magnitudes and signs of the wavelength shift as the samples are bent; (c) the same set of wavelength shift data in Fig. 8(b) re-plotted as a function of local strain at the resonators. The solid line is the theoretical prediction of Eq. (2) based on finite element strain distribution simulation results.

Optomechanical coupling in flexible photonic resonators has been investigated by several groups [16, 40, 86]. For resonators made of the same material and of the identical dimensions, Eq. (2) suggests the same $d\lambda/d\varepsilon$ coefficient regardless of the flexible device configuration. This conclusion was experimentally validated by our *in situ* transmission measurement of flexible micro-disk resonators [40]. Figure 8(a) shows a flexible micro-disk resonator chip under testing: optical transmission through the bus waveguides was monitored *in situ* using

#191249 - $15.00 USD Received 31 May 2013; revised 31 Jul 2013; accepted 2 Aug 2013; published 12 Aug 2013

fiber end fire coupling as the flexible chip is bent. The resonant wavelength shift as a function of bending radius was measured on several different samples with different top/bottom cladding layer thickness combinations and is plotted in Fig. 8(b). While Fig. 8(b) indicates that the resonant wavelength shift may differ significantly in both magnitude and sign as the device configuration changes, re-plotting the same set of data as a function of local strain at the micro-disk resonators (Fig. 8(c)) clearly shows that all data points nearly fall on a straight line which agrees well with Eq. (2).

In the example shown in Fig. 8, the main contribution to resonant wavelength shift comes from the strain-optic material response. Due to the relatively small strain-optic coefficient of most engineering materials, tuning relying on photoelastic property change of materials (i.e. the first RHS term in Eq. (2) is inherently limited in tuning range. Broadband tuning has been accomplished on flexible photonics platforms by mechanical deformation of the cavity geometry (i.e. the second and third RHS terms in Eq. (3). Yu *et al.* demonstrated a stretchable photonic crystal cavity with over 60 nm wavelength tuning range near 1550 nm telecommunication wavelength (Fig. 9). The PhC consisted of a hexagonal array of Si rods, and the line defect cavity was formed by reducing the diameter of 19 rods along a line. The PhC was embedded in PDMS elastomer which rendered the structure mechanically compliant. When stretched, the cavity length changes leading to a resonant wavelength shift. The high yield limit of PDMS accounts for the large 67 nm wavelength tuning range, which well exceeds other existing tuning mechanisms. The maximum tuning range in a stretchable PhC cavity is ultimately limited by degradation of optical confinement and cavity Q-factor as the PhC geometry is deformed. The same mechanism has also been implemented to tune the optical resonant wavelength of metamaterials [88] and surface plasmon polaritons [89].

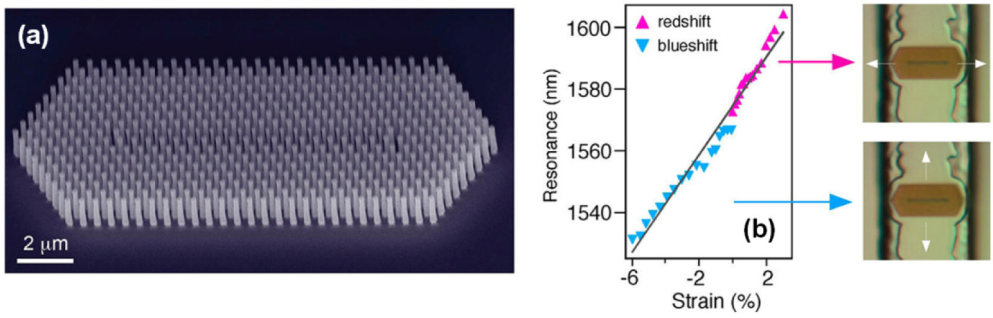

Fig. 9. (a) SEM image of a photonic crystal cavity comprising a hexagonal array of silicon nanowires; the PhC was subsequently infiltrated with PDMS elastomer to form the stretchable cavity; (b) cavity resonance shift under mechanical stretching as a function of strain along the cavity, where strain is defined as the percentage change of the cavity length. Two stretching directions were explored (optical images): along or orthogonal to the line defect (image courtesy of [14]).

Besides resonant wavelength tuning, mechanical deformation was also used to modulate optical coupling by varying the gap width between photonic elements. The technique was applied to tune Mach-Zehnder interferometers and micro-ring resonators by Chen *et al.* [13].

4.3. Flexible detector/LED arrays

LED array integration on plastic substrates is a key enabling technology for flexible displays used in consumer electronics. Mechanical flexibility, on the other hand, allows the assembly of non-planar imaging arrays with hemispherical Field of View (FoV), low aberration, and conformal integration capability on complex curvilinear surfaces [2, 90].

We have developed a frame-assisted membrane transfer (FAMT) process for the transfer of large-area crystalline semiconductor NMs, especially for the fragile material systems such as GaAs and InP compound semiconductors used inflexible detector and LED fabrication

#191249 - $15.00 USD Received 31 May 2013; revised 31 Jul 2013; accepted 2 Aug 2013; published 12 Aug 2013

[38]. Large area flexible photodetectors, solar cells and LED arrays all have been demonstrated experimentally, as shown in Fig. 10, based on transferred InP nanomembranes. The measured flexible InP p-i-n photodetector performance characteristics under bending (bending radius = 32.3 mm) are shown in Fig. 11(a). Dark current of 1 μA was obtained for a 3 × 3 mm^2 device. The measured current-voltage curve for the flexible InP solar cell under bending (bending radius = 42.1 mm) is shown in Fig. 11(b). We obtained photovoltaic solar cells with open circuit voltage of 0.62 V, and power efficiency of 1.44%. Higher efficiency cells are feasible with optimized structural design by optimal absorption, light trapping, and photon recycling.

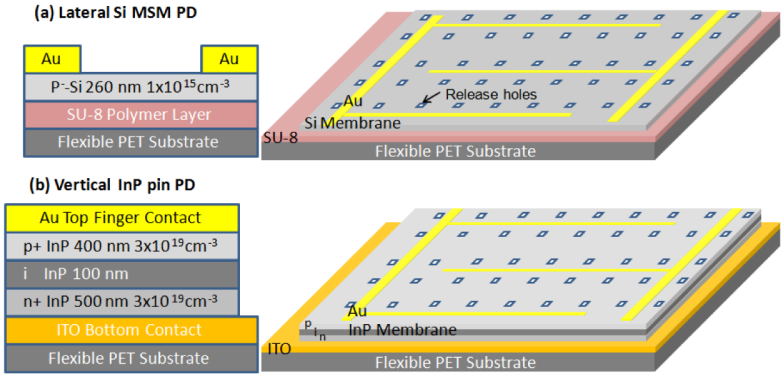

Fig. 10. Schematics of (a) a lateral Si MSM photodetector (PD), and (b) a vertical InP p-i-n photodetector, based on transferred crystalline semiconductor nanomembrane processes (image courtesy of [39]).

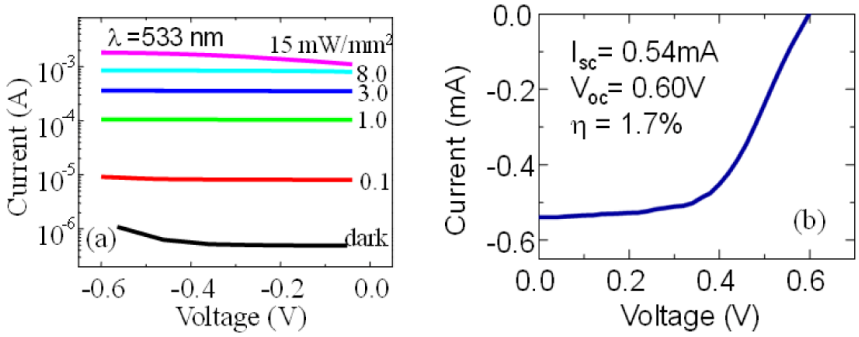

Fig. 11. (a) Flexible InP photodetectors under bending: measured photocurrent with 533 nm light sources at different optical power; and (b) Flexible InP solar cells under bending: measured current under standard AM solar simulator test conditions at room temperature (image courtesy of [39]).

We also demonstrated 8 × 8 flexible InP LED arrays, based on a modified transfer process. The starting wafer is InGaAsP QW Cavity wafer comprising of the device layers (top and bottom contact layers, cladding and spacer layers on top and bottom, and quantum well (QW) structures in the middle) grown on top of the sacrificial layers (e.g., InP and InGaAs for the InP material system). The top rings are first patterned into various diameter sizes of mesas with 5 μm-wide, using optical lithography. The top ring metal contacts are defined by electron-beam evaporation (Pd/Zn/Pd/Au: 10/10/20/200 nm) on top surface of source wafer and then liftoff. Next, an alignment pattern to protect metal contacts is patterned before the regions between the metal contacts of active layer are selectively etched down to the bottom

#191249 - $15.00 USD Received 31 May 2013; revised 31 Jul 2013; accepted 2 Aug 2013; published 12 Aug 2013

contact layer with wet chemical etching. In our case, the InGaAs and InGaAsP QW layers are selectively etched away by the chemical mix of $HF/H_2O_2/H_2O$ (1:1:10) solution and The InP layer is selectively etched away by the chemical mix of HCl/H_3PO_4 (1:4). The bottom contact patterns are formed into stripes by photolithography and subsequent evaporation of metals (Ni/Ge/Au/Ti/Au: 15/20/30/10/100 nm) at the bottom of the etched regions and then liftoff. The thin PECVD SiO_2 layer with total thickness of 600 nm was universally deposited to passivate all devices. The devices are patterned and access holes of both top and bottom contacts are formed by photolithography and passivated layer is etched by using the RIE-etching. Finally, the interconnect layer was patterned to connect all of the devices together forming the device arrays. A completed flexible InP LED arrays were formed, with top and bottom contacts (Fig. 12(a)). The SEM image of top ring contact and interconnect line connecting to the stripe to form the arrays and laying on the SiO_2 passivation layer is shown in Fig. 12(b). The InP LED was transferred onto flexible PET substrate as shown in Fig. 12(c). In Fig. 12(d) shows the device was under probing test and Fig. 12(e) illustrates the device was transferred onto gold coated PET substrate.

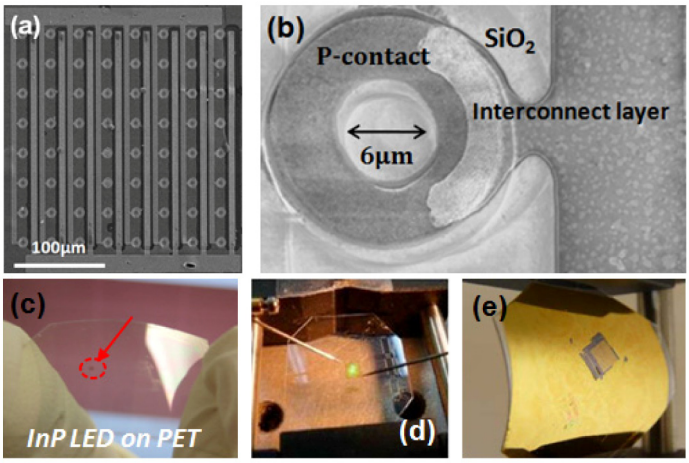

Fig. 12. Demonstration of flexible LEDs based on InGaAsP QW NM transferred onto PET substrates. (a) SEM images of 8 by 8 devices on PET substrate after testing. (b) SEM image of top ring contact linked by interconnect layer and passivated by a SiO_2 layer. (c) Image of devices transferred onto PET substrate. (d) Image of devices under probing test. (e) Image of fabricated devices on Au coated PET substrate (image courtesy of [62]).

4.4. Sensing systems integrated on biological tissues

Many reports appeared over the last year, in the area of NM-based bio-integrated flexible devices and systems, where high-performance semiconductor device functionality can be achieved in forms that enable intimate, conformal contacts to flexible/conformal surfaces. Kim *et al.* presented a flexible/stretchable systems of InGaN microscale transfer printed inorganic LEDs (m-ILEDs) with wireless powering schemes, for implantable devices that could be used to accelerate wound healing, activate photosensitive drugs, or to perform imaging and spectroscopic characterization of internal tissues [91–93]. One of the more sophisticated examples of flexible optoelectronics in biology was demonstrated in a recent paper, where tiny LEDs were injected into the brains of mice to provide wireless control over behavioral responses through optogenetic techniques [94]. Along the direction of bio-integrated optoelectronics, a physically transient form of silicon electronics was proposed [95], where nanomembrane devices are built on bio-resorbable substrates (e.g. silk) and the complete material system disappears physically at prescribed times and at controlled rates. An

#191249 - $15.00 USD Received 31 May 2013; revised 31 Jul 2013; accepted 2 Aug 2013; published 12 Aug 2013

implantable transient device that acts as a programmable non-antibiotic bacteriocide was demonstrated and sealed in silk packages.

5. Challenges, opportunities, and future trends

Even though flexible integrated photonics is still in its infancy, many exciting applications have already been demonstrated as noted in the previous section. New materials and processing methods, as well as innovative optical and mechanical device designs are expected to further improve the performance of flexible photonic systems. To name a couple of examples, roll-to-roll manufacturing of flexible photonic structures will enable device fabrication over large substrate areas inaccessible using conventional processing techniques on rigid substrates, and integration of flexible photonic elements with MEMS actuating systems can lead to novel tunable photonic devices exploiting their singular strain-optical coupling behavior.

While flexible photonics offers a unique platform to explore strain-optical coupling for photonic tuning, such coupling is undesirable or even harmful for other applications where stable device operation independent of substrate geometry is essential (e.g. for sensing systems integrated on biological tissues). Controlling the coupling via nano-mechanical designs (e.g. multi-layer designs implemented in Fig. 8(b), or locally stiffened islands to minimize deformation of devices) is thus critical for practical applications of flexible photonic systems.

Optical coupling into and out of flexible photonic devices (in particular waveguide-based devices) presents another remaining technical challenge for flexible photonics. Grating coupling and butt coupling have both been employed, although both coupling scheme severely limit the deployment degrees of freedom of flexible photonic systems. Complete photonic integration of both active and passive elements (and possibly with power sources) on flexible substrates will significantly simplify system packaging and is highly desirable for many of the aforementioned applications, although careful thermal designs are required to mitigate the heat dissipation issue especially for free-standing flexible photonic systems where heat sinks are not readily accessible.

6. Concluding remarks

In this paper, we reviewed the material design, mechanical engineering, and photonic applications of flexible integrated photonics. We show that the requirement for structural flexibility and stretchability can be decoupled from its constituent material mechanical properties through ingenious nano-mechanical designs. Therefore, mechanically compliant structures can be made out of materials that are rigid in their bulk form. For example, crystalline semiconductor NMs, the key enabling material for flexible electronics, are also the material of choice underlying flexible active optoelectronic device applications, while amorphous glasses are promising candidates for passive optical components. Based on these novel materials and innovative device designs, flexible integrated photonics has found niche applications for interconnects, sensing, imaging, and photonic tuning. We anticipate that identification of new application fields where mechanical flexibility either constitutes the key feature enabling the target applications or contributes to significantly improved device performance will certainly accelerate penetration of the technology into diverse market sectors in the future.

Acknowledgments

The authors thank Shutao Qiao and Dr. Nanshu Lu at the University of Texas at Austin for performing the finite element simulations and helpful discussions. L. L. acknowledges funding support from Delaware NASA/EPSCoR through the Research Infrastructure Development (RID) grant. J. H. and H. L. acknowledge partial funding support from the National Science Foundation under award number 1200406. P. Z. acknowledges financial

support provided by the China Scholarship Council (No: 201206255016). W. Z. and Z. M. acknowledge the funding support from US AFOSR (FA9550-08-1-0337 and FA9550-09-C-0200) and from US ARO (W911NF-09-1-0505). The AFOSR program manager is Dr. Gernot Pomrenke and the ARO program manager is Dr. Mike Gerhold.

#191249 - $15.00 USD Received 31 May 2013; revised 31 Jul 2013; accepted 2 Aug 2013; published 12 Aug 2013